Multi-Material Topology Optimization in LS-TaSC™ Using Ordered SIMP Interpolation

Satchit Ramnath[1], Mariusz Bujny[2], Nathan Zurbrugg[3], Stefan Menzel[2], Duane Detwiler[3]

[1]*SIMCenter, The Ohio State University, Columbus, Ohio, USA*
[2]*Honda Research Institute Europe GmbH, Offenbach/Main, Germany*
[3]*Honda Research & Development Americas, Raymond, Ohio, USA*

Abstract

Topology optimization allows for the design of structures with an optimum distribution of material for a given set of load cases that may have conflicting requirements. Though the methods used in topology optimization help to generate better and novel designs, they are generally limited to a single material only. In contrast, modern vehicle structures are composed of parts made of multiple materials, exhibiting usually superior performance compared to single-material designs. In order to support the design process of such structures, this problem requires the ability to use multi-material optimization methods within commercially available software like LS-TaSC, to optimally distribute multiple materials within a single design domain. In this paper, a method for integration of the ordered SIMP in LS-TaSC to realize multi-material TO is proposed and evaluated using a solid beam that is subject to static and crash load cases. The optimization uses the updated material distribution, based on ordered SIMP, to assign material/density values to elements in the design domain. To demonstrate the potential of the multi-material TO and validate the results, the obtained topologies are compared to single material designs as well as to the structures optimized using the state-of-the-art gradient-based approach based on ordered SIMP. The results show that LS-TaSC can be successfully used for deriving multi-material structures superior to the single-material designs. Finally, due to the low computational costs, the method seems to be suitable for the optimization of large-scale industrial models.

1. Introduction

The use of Topology Optimization (TO) in the automotive industry has proven to be an effective tool for developing conceptual designs capable of meeting conflicting requirements like stiffness, safety, and light weighting. During the last years, the design process in the automotive industry has been changing very dynamically thanks to the utilization of TO [1][2][3][4] and related post-processing techniques [5]. TO is a mathematical method used to optimize the material layout within a defined design space, for a given set of boundary conditions like loads or supports. The complexity of the automotive structures is increasing with every generation update. Thus, the updated designs are required to satisfy quickly changing, and sometimes conflicting, requirements from various disciplines in the development cycle.

To meet challenging requirements like weight and cost for modern vehicles, structures composed of parts made of different materials became a standard in the automotive industry. As a consequence, multi-material TO approaches which are able to determine not only the distribution of material within the design space, but also the splitting into different material types, are gaining more and more attention recently. In particular, density-based multi-material TO methods, which are interesting from the perspective of this work, can be divided into the following four groups: SIMP-based methods using multiple variables for encoding each material type [6], phase-field methods [7], alternating active phase approaches [8], and ordered-SIMP-based methods [9][10]. The main disadvantage of the three first groups of methods is the fact that the computational costs rise considerably when the number of materials increases, which might be a severe limitation in case of application of these methods in the industrial setting, where usually a high number of material types is taken into consideration. The phase field methods are very complex, exhibit problems with numerical instabilities [9], and usually require a high number of iterations to converge (over 10^4 iterations are frequently necessary to find a suitable solution [11]).

What is more, the first three groups of methods involve significant modifications of the underlying TO approach, which makes their implementation in a black-box TO software, like LS-TaSC, difficult. In contrast, the ordered SIMP approach relies on the modification of the material interpolation scheme, and therefore, can be more easily integrated into commercial TO software. Since a single design variable is used to encode both, the material density as well as the material type for each finite element, the computational costs do not increase compared to standard TO methods even for a large number of different materials. Finally, initial studies [10][12] showed that ordered SIMP can be integrated into non-gradient TO approaches such as Hybrid Cellular Automata (HCA) [13] and can be successfully used in optimization of structures under crash loads. As a result, in this paper, we propose to use ordered SIMP to enhance the capabilities of LS-TaSC in order realize multi-material TO of large-scale industrial cases under static and crash load cases.

The paper is organized as follows: Section 2 provides more details about the ordered SIMP method. Section 3 explains the integration of this method with LS-TaSC. Section 4 details the test case used to demonstrate the process. Section 5 and 6 discuss the results obtained from the simulations. The paper is concluded in Section 7 along with potential future research directions.

2. Topology Optimization using Ordered SIMP

Ordered SIMP approach was first proposed by Zuo and Saitou [9] as an interpolation scheme for multi-material, gradient-based TO of linear elastic structures under static loads. At first, for m material types of mass density $\rho_i^T, i = 1,2,3, \dots, m$, the method requires the definition of the corresponding normalized densities according to the following formula:

$$\rho_i = \frac{\rho_i^T}{\rho_{max}^T} \ (i = 1,2,3, \dots, m), \tag{1}$$

where ρ_{max}^T is the highest mass density out of the all considered materials. The densities are sorted in ascending order, i.e. $\rho_1 < \rho_2 < \dots < \rho_{m-1} < \rho_m$. Subsequently, the classical single-material SIMP scheme [6] is modified as follows:

$$E_e(\rho_e) = A_E \rho_e^p + B_E, \tag{2}$$

where ρ_e^p is a (penalized) normalized density of the finite element e, with a penalization exponent p. The element densities $\rho_e, e = 1,2, \dots, n$, with n being the total number of finite elements, are the design variables for the optimization problem. E_e is the resulting Young's modulus and the coefficients A_E and B_E for $\rho_e \in [\rho_i, \rho_{i+1}]$ are given as:

$$A_E = \frac{E_i - E_{i+1}}{\rho_i^p - \rho_{i+1}^p}, \tag{3}$$

and:

$$B_E = E_i - A_E \rho_i^p, \tag{4}$$

where E_i is the Young's modulus of the ith material. Figure 1 shows the ordered SIMP interpolation according to Equation (2), with $p = 3$, for three material types: void ($\rho_1 = 0$, $E_1 = 0$), aluminum ($\rho_2 = 0.36$, $E_2 = 0.367$), and steel ($\rho_2 = 1.0$, $E_2 = 1.0$). For simplicity, we considered normalized density and Young's moduli values only. Please note that the design variable ρ_e does not only determine the Young's modulus values, but also encodes the material type. As a result, no additional parameters are needed to realize multi-material TO.
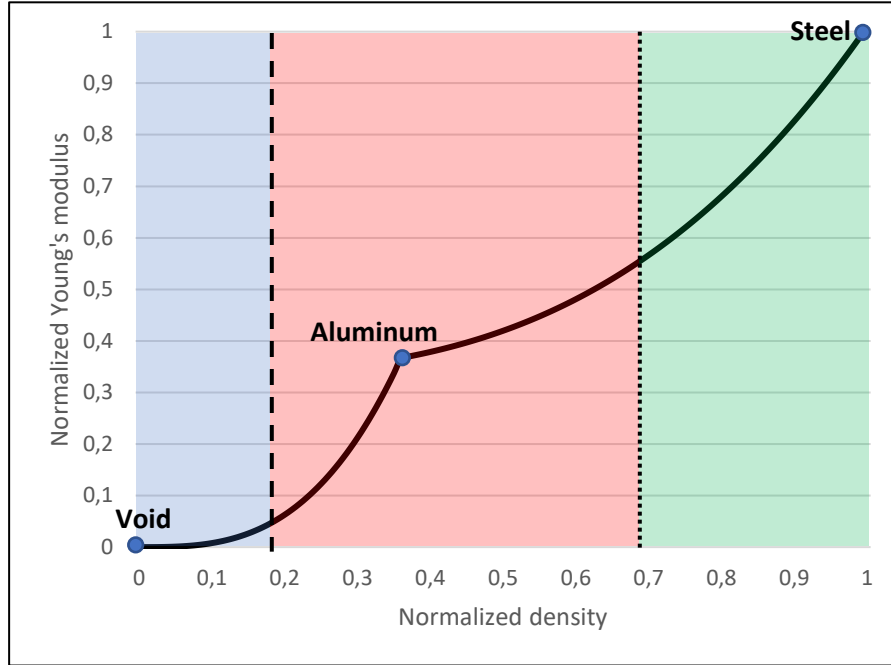
Figure 1: Relationship between normalized Young's modulus and normalized density according to the ordered SIMP scheme, for an optimization problem with three material types: void, aluminum, and steel. The elements of densities in range [0, 0.18] are interpreted as void (blue area), in (0.18, 0.68] range as aluminum (red area), and in (0.68, 1.0] range as steel (green area). The density ranges are determined based on Equation (5).

One can easily see in Figure 1 that the Young's modulus values are penalized in the intermediate density ranges. More precisely, only for the normalized densities of ρ_1, ρ_2, and ρ_3 the Young's modulus takes true values and everywhere else it is more than proportionally reduced. As a result, the optimizer, targeting efficient utilization of material for a fixed mass fraction, will tend to distribute the material around the densities corresponding to the three different material types. However, since the intermediate densities can still appear in the optimized structures, we propose to post-process the resulting densities according to the following rule:

$$\rho_e^F = \begin{cases} \rho_1, & if\ \rho_e \in \left[\rho_1, \dfrac{\rho_1 + \rho_2}{2}\right] \\ \rho_2, & if\ \rho_e \in \left(\dfrac{\rho_1 + \rho_2}{2}, \dfrac{\rho_2 + \rho_3}{2}\right] \\ \rho_3, & if\ \rho_e \in \left(\dfrac{\rho_2 + \rho_3}{2}, \rho_3\right] \end{cases} \tag{5}$$

where ρ_e^F is the final, post-processed density of the finite element e. The density thresholds $\frac{\rho_1+\rho_2}{2}$ and $\frac{\rho_2+\rho_3}{2}$ are marked using dashed and dotted lines in Figure 1, respectively. After the post-processing stage, only the three predefined material types are present in the design used for the final evaluation of performance.

The gradient-based ordered SIMP [1] involves rigorous derivation of sensitivities for the interpolation scheme (2) and modifications of the Optimality Criteria (OC) method, used to solve the optimization problem. These steps are not necessary for the implementation of the method in non-gradient approaches (e.g. HCA) or LS-TaSC, and therefore are not discussed in this paper. Nevertheless, in this work, an in-house Python implementation of the ordered SIMP as proposed by Zuo and Saitou [9] is used to validate the results obtained with the method proposed in the next section.

3. Integrating Ordered SIMP with LS-TaSC

The TO set up, in terms of load cases, is similar to a regular set up for a single material optimization using SIMP in LS-TaSC. The material card that stores the distribution for two materials is created using a separate script file that penalizes the material densities and, in this case, Young's modulus. This is done using the method based on Equation (2) from the previous section and illustrated in Figure 1.

During runtime, LS-TaSC creates the material card for a TO which holds the density values for the material to be used in optimization. The name of the file storing the material data is *lst_mat.k* and is saved in the project folder. In the case of multi-material optimization using Ordered SIMP, the material card generated by the script is used to replace the original material card written out by LS-TaSC within the project folder. The replacement of material card/file is automated at runtime using a shell script.

An important thing to note is that LS-TaSC by default (when using projected sub-gradient method) tries to get rid of intermediate density elements and pushes the elements to either 0 (no material) or 1 (full density). However, for the ordered SIMP method to work, LS-TaSC is required to retain intermediate density elements due to the unique nature of the material model, which in this case corresponds to different material types of a full density. This can be achieved by switching the optimization algorithm to *Optimality Criteria* in LS-TaSC and changing the toggle in settings to retain intermediate density elements. In the case of using LS-TaSC to solve for multiple load cases involving static and crash loads, the weighting is done using the scaled energy weighting method (SEW-LS-TaSC) [14] inspired by the SEW-HCA approach [15].

4. Case Study on a Beam Model

In this paper, the method described to integrate the Ordered SIMP approach with LS-TaSC is demonstrated using a beam model [14]. The beam model is optimized for two different objectives (minimum compliance and maximum energy absorption) in two load cases, as discussed in detail below. The finite element model is developed in LS-DYNA® keyword format. The static load case is analyzed using the implicit solver while the load case for energy absorption is solved using the explicit solver in LS-DYNA. The material model for the static case is linear elastic and for the crash case is piecewise linear elastic-plastic. The elastic and plastic properties for two materials, aluminum and steel, are defined to be used in the simulations. For the elastic region, density, Young's modulus and Poisson's ratio are defined, whereas, the plastic regions are defined by a bilinear curve, using the tangent modulus.

The beam model is setup as a simply supported beam problem with two load cases. Figure 2 shows the constraints utilized for setting up the model used in the paper. The design space of the beam model contains 12,000 voxel elements as shown in Figure 3.
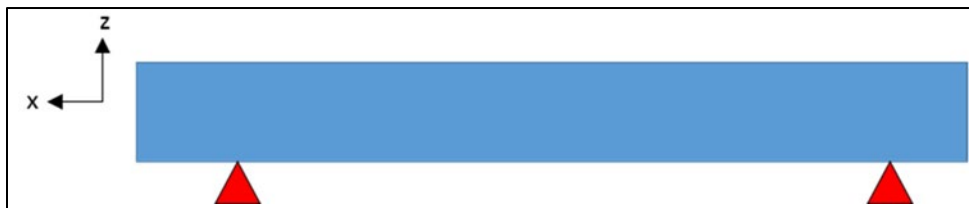

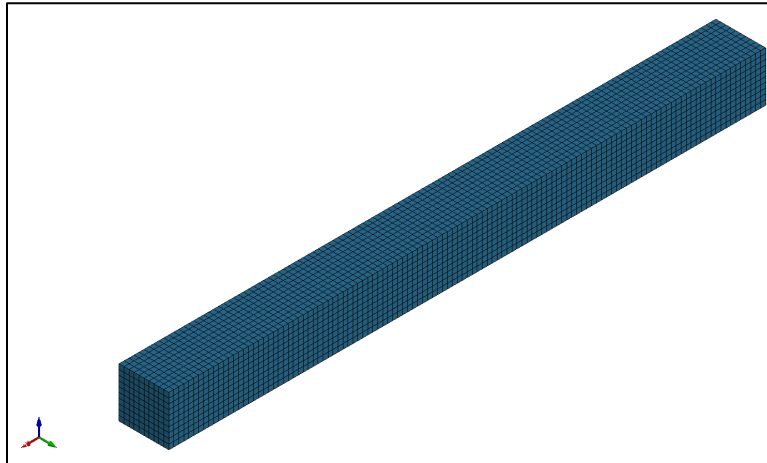Figure 2: Simply Supported Beam

Figure 3: Voxelized Beam Model

The first load case is a dynamic crash scenario shown in Figure 4, in which the optimization objective is to maximize the energy absorption from the indenter. The cylindrical indenter is forced into the beam, along the z-direction, to create significant deformation. The motion of the indenter is defined as a linear motion with a constant velocity of 100 mm/s, until a displacement of 100 mm is reached. This is applied within LS-DYNA using the BOUNDARY_PRESCRIBED_MOTION card. In the second load case, a point static load of 1000 N is applied in the y-direction (Figure 5). The optimization objective for this case is to minimize compliance.
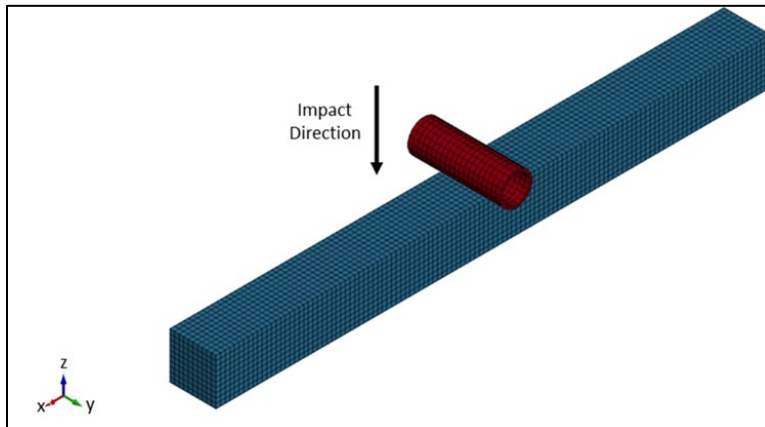
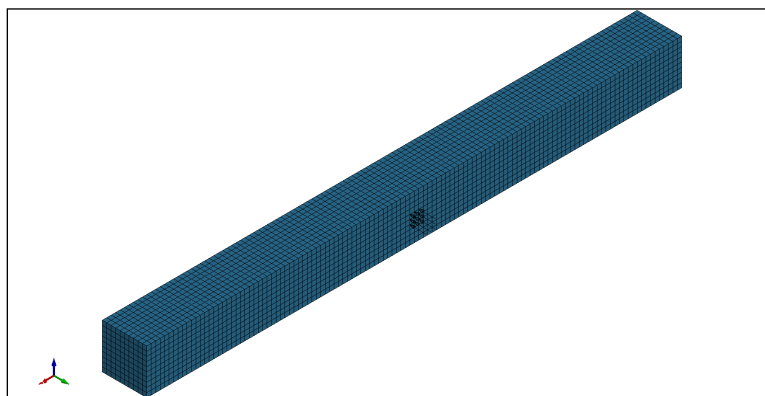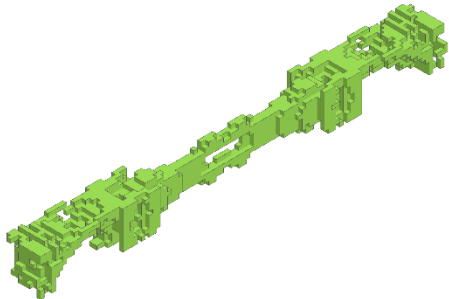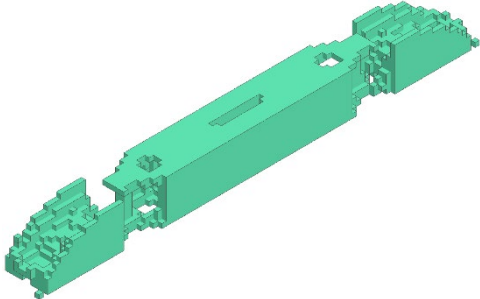Figure 4: Dynamic Load Case Setup
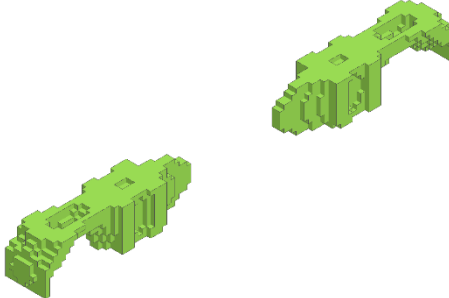
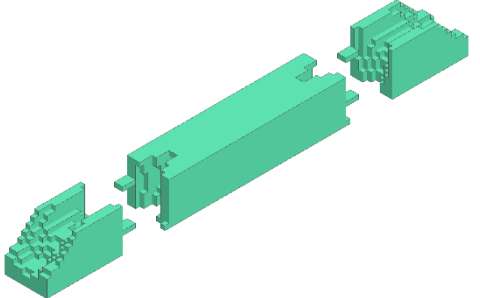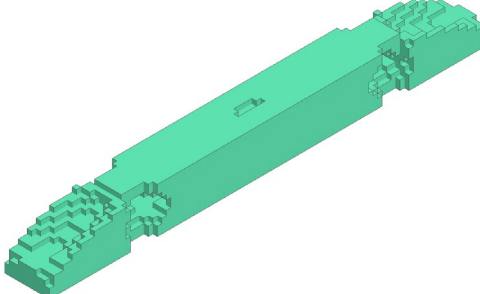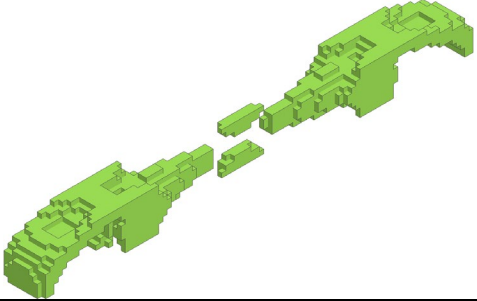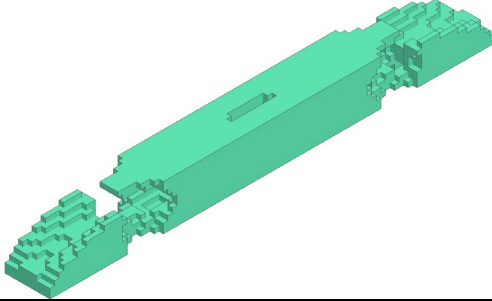Figure 5: Static Load Case Setup

5. Comparison of LS-TaSC and gradient-based Ordered SIMP

In order to validate the proposed multi-material TO approach based on LS-TaSC, we consider first the static test case described in Section 4. The structure is optimized for minimal compliance under 60% mass constraint. For comparison, the same optimization problem is solved using the in-house implementation of the gradient-based ordered SIMP approach [9] as well as the classical, single-material SIMP method [6]. After the optimization, all of the designs are post-processed, to eliminate intermediate densities and obtain clear definitions of aluminum and steel regions. Additionally, to demonstrate the usefulness of the ordered SIMP interpolation scheme, we interpret the elements with intermediate densities from the single-material SIMP optimization as steel and aluminum parts, using the same post-processing approach. The structures after post-processing have to meet the 60% mass constraint. Subsequently, the performance of the structures is evaluated again and used for the comparison of the methods. The compliance values, normalized w.r.t. the LS-TaSC Ordered SIMP result, as well as distributions of materials, are given in Table 1.

Table 1: Comparison of compliance values and distributions of materials for designs optimized using the novel LS-TaSC Ordered SIMP approach, gradient-based Ordered SIMP [9], and the standard, single-material SIMP [6]. Additionally, in the last row, the intermediate densities from the standard SIMP have been interpreted as aluminum and steel by following the post-processing approach used in Ordered SIMP. All of the structures have the same mass (difference less than 0.3%).

Method	Normalized compliance	Aluminum part	Steel part
LS-TaSC Ordered SIMP	1.0		
Gradient-based Ordered SIMP	1.01		
Standard SIMP	1.05		

Standard SIMP for multi-material TO	1.19		

The compliance values obtained with the LS-TaSC Ordered SIMP method and the gradient-based Ordered SIMP are very close, differing by ca. 1%. Surprisingly, the structure obtained with our LS-TaSC Ordered SIMP approach is slightly stiffer. The distributions of aluminum and steel are qualitatively similar for both methods, but not identical. One can also easily see more checkerboard-like patterns on the boundaries between different material phases for the design obtained with the LS-TaSC Ordered SIMP approach, which is a known problem of the methods based on ordered SIMP interpolation [9]. These effects are stronger for the LS-TaSC Ordered SIMP implementation probably due to the lack of tuning of the optimization method itself to the new interpolation scheme. Please note that our approach is based on a simple replacement of a file with material cards, while Zuo and Saitou [9] propose specific modifications both to the OC algorithm as well as the hyperparameters of the method.

Compared to the single-material design obtained with the standard SIMP approach [6], which is shown in the third row of Table 1, both multi-material structures are significantly stiffer, with LS-TaSC Ordered SIMP design reaching a 5% lower compliance value. This shows the potential of multi-material designs in improving the structural performance and demonstrates the validity of the proposed method. One should also note that by a simple interpretation of intermediate densities obtained with the standard SIMP as different materials, inferior designs would be usually obtained, and the use of the modified interpolation scheme (2) is absolutely necessary. This is also the case for the structure presented in the last row of Table 1, which was generated with use of the multi-material post-processing technique based on the single-material structure obtained with SIMP. The post-processed structure has almost 20% higher compliance than the LS-TaSC Ordered SIMP design, which demonstrates the usefulness of the ordered SIMP interpolation.

6. Multi-objective multi-material TO for crash and statics with LS-TaSC

In this section, the results for MMTO on the beam model is presented based on the ordered SIMP approach in LS-TaSC. The TO is done with varying preference values [15][16] for the load cases and different materials. This includes two LS-TaSC setups for single material topology optimization (SMTO) with steel and aluminum, and one setup for multi-material topology optimization (MMTO) with an aluminum-steel combination. A target mass fraction of 30% is set along with a move limit of 0.1. The results obtained from the optimization run can be used as a starting point for the further design development process. The material card for SMTO is obtained using the traditional SIMP formulation while the material card for MMTO is produced using the Ordered SIMP approach given by (2) as described in the previous section. The TO runs are performed using the LS-OPT® workflow [14].

Figure 6, 7, and 8 show the Pareto front obtained for the two load cases considered in the case study. On the y-axis is the internal energy (IE) for the static case and on the x-axis is the IE for the crash case. For the static load case the IE is proportional to compliance and hence the objective is to minimize the IE while for crash, the objective is to maximize IE. Each square in the Pareto front corresponds to a particular set of preference values for each load case, generated using the Design of Experiments (DOE) method (space filling) in LS-OPT. Selecting the data point within an acceptable range of internal energies, would give the desired conceptual design. The bottom most and topmost points in the Pareto fronts represent the designs with static dominant and crash dominant preferences respectively. The one in the middle is the design obtained for equal preferences to both the load cases.

The optimization algorithm fills the inside with a softer material, making it less stiff and more energy absorbent, as the preference moves from static towards crash, and steel is present on the outside to provide for stiffness of the beam. Figure 8 (Pareto front for MMTO) shows the distribution of aluminum and steel in the beam model after MMTO.
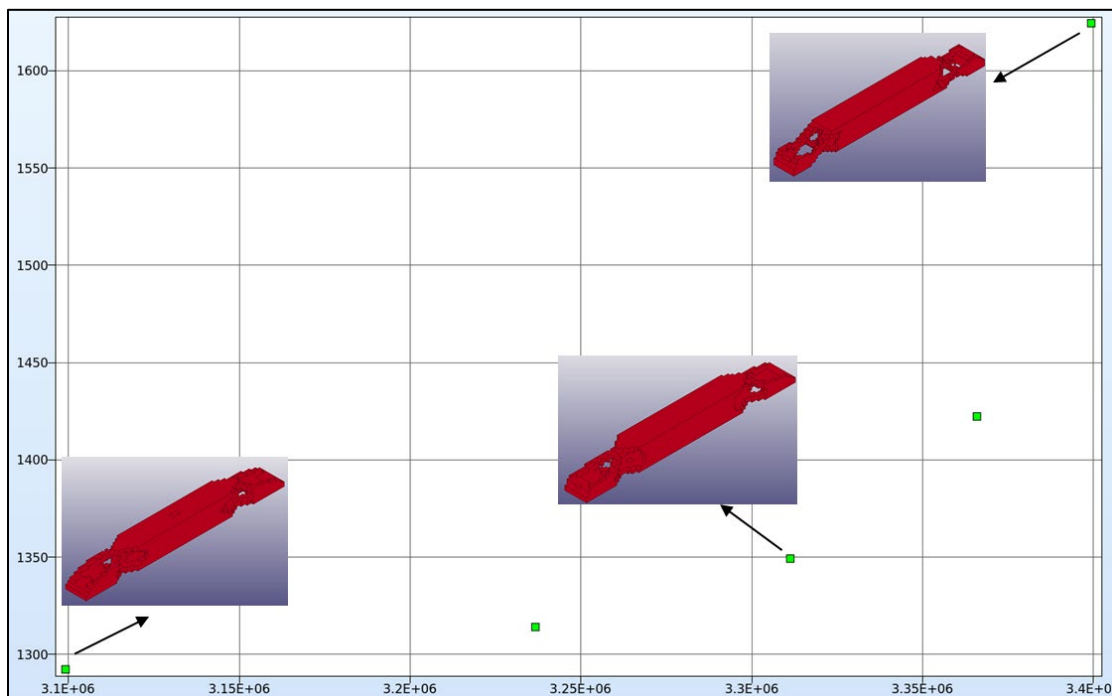

Figure 6: Pareto Front obtained from SMTO (aluminum). y axis: IE for static case; x-axis: IE for crash case.
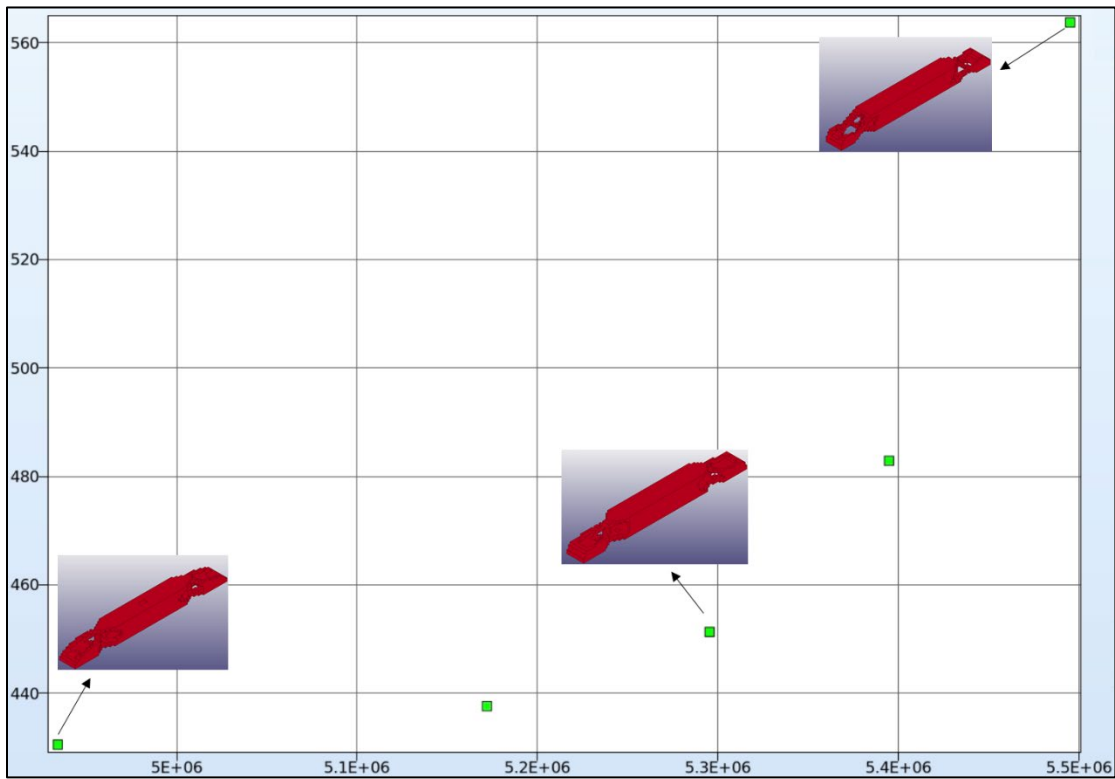
Figure 7: Pareto Front obtained from SMTO (steel). y axis: IE for static case; x-axis: IE for crash case.
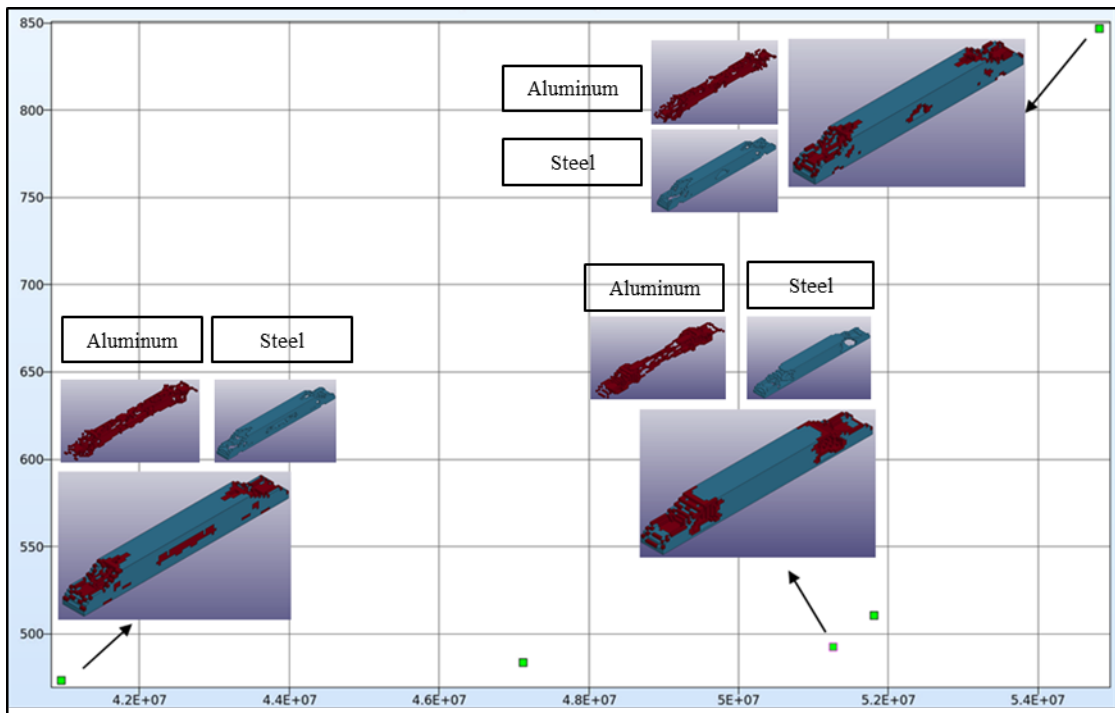

Figure 8: Pareto Front obtained from MMTO (aluminum-steel). y axis: IE for static case; x-axis: IE for crash case.

Figure 9 shows the comparison of the Pareto fronts for all three cases (SMTO - aluminum, SMTO - steel and MMTO aluminum-steel). The y and x axes are the normalized internal energies for the static and crash load cases respectively. From the figure, it can be noted that the MMTO model performs much better than both the SMTO models since it absorbs a lot more energy, while the performance in the static case is good and comparable to that of the SMTO – steel model.
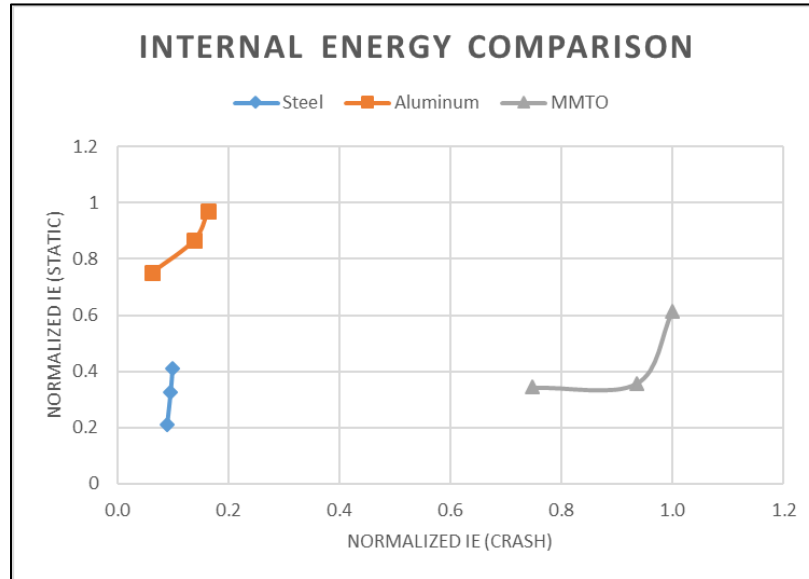

Figure 9: Internal Energy Comparison

The individual performances (based on internal energy) of the optimized model for SMTO and MMTO for various material models can be seen in Figure 10. The vertical axis represents the internal energy in the crash or static load case and horizontal axis represents the preference parameter. The left most point (0.1 preference) shows the least preference given to that particular load case and the right most point (0.9) is for most preference. For the crash load case, a higher internal energy signifies a better model since it absorbs more energy and for the static load case, a lower internal energy values is preferred, since it implies that the model is stiffer, thereby having a lower compliance.

In Figure 10 the internal energy vs preference parameter for the crash load case, the internal energy is higher for the MMTO when compared to the two SMTO cases, especially when the preference for the crash case is set within the range of 0.5 to 0.9. The significantly higher internal energy in the MMTO cases suggests that the energy absorption is also higher. Similarly, for the static load case, the internal energy for the MMTO case is lower than SMTO for aluminum and quite comparable to the SMTO for steel case. This trend suggests that the MMTO better meets the minimum compliance requirement especially when the preference is within the range of 0.5–0.9.
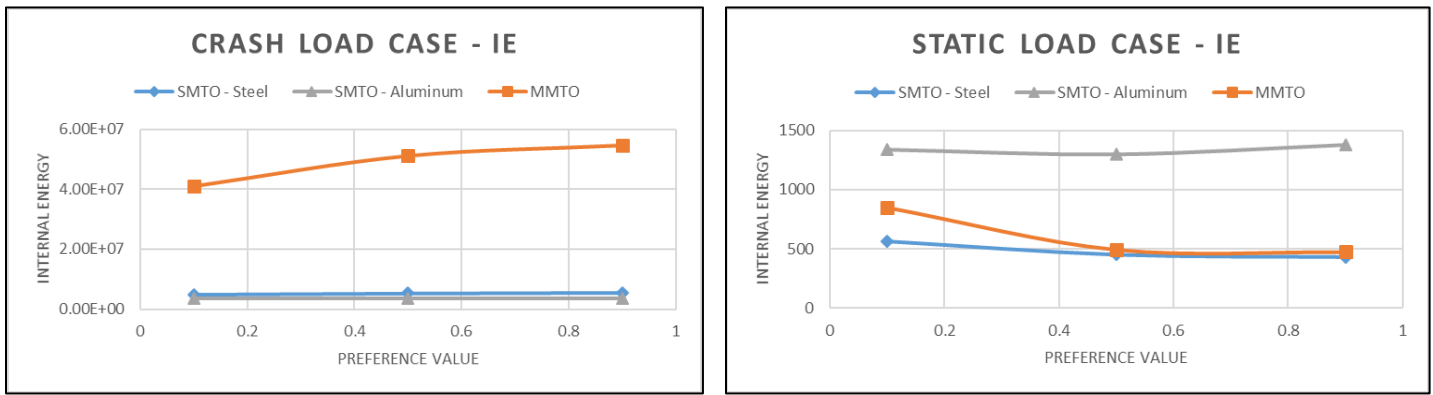
Figure 10: IE vs preference for both load cases (crash – left and static – right)

For the results obtained from MMTO figure 11 shows an example for individual material distribution for both materials. The full density material assignment for aluminum and steel is done based on the thresholds mentioned in Section 2. The static and crash load cases have equal preference values (0.5, 0.5) in this case. The material distribution is such that the softer material (aluminum) is in the interior and stiffer material (steel) on the outside.
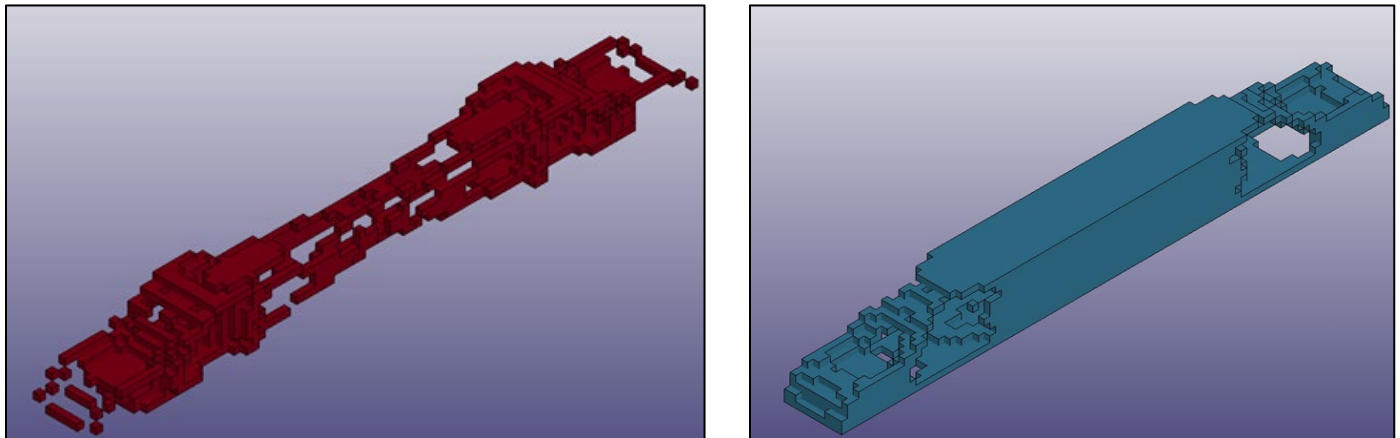

Figure 11: Material Distribution for Aluminum (left) and for Steel (right)
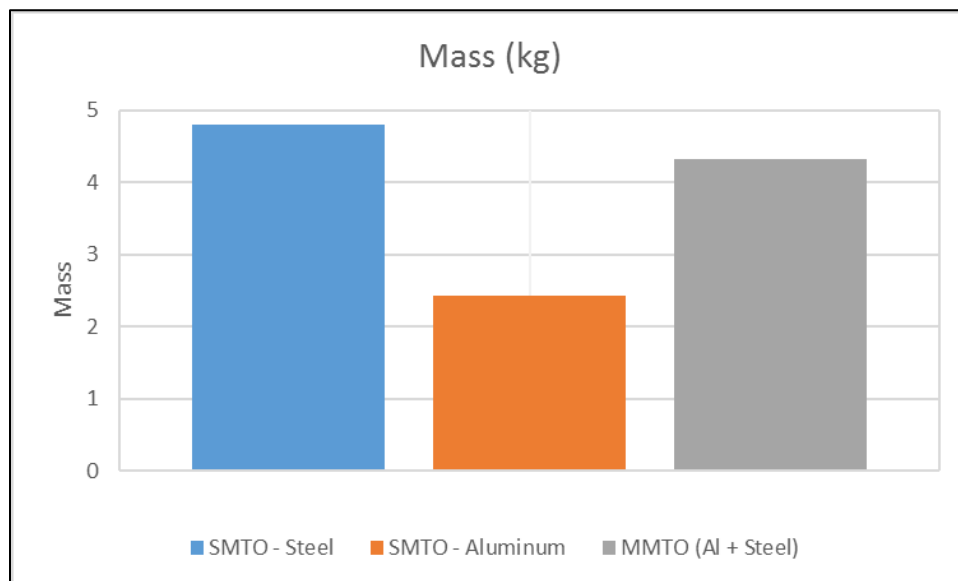

Figure 12: Average mass of optimized models for various preferences

The results from the SMTO and MMTO are post-processed based on the density thresholds discussed in (5) of Section 2. The post-processed model is the one with full density assigned to the elements. Figure 12 compares the average mass of the optimized model from SMTO (steel and aluminum) and MMTO models for various preferences (Steel: 4.8kg, Al: 2.5kg, Steel + Al: 4.3kg). The mass of the model obtained from MMTO falls within a reasonable range in between the mass of the models from SMTO.

7 Discussion

For linear elastic materials, the *updated* material model is formulated using the density and Young's modulus of the desired materials as discussed previously in Section 2. However, in the case of crash behavior, it is important to consider the large deformations and plastic behavior of the materials. An approach similar to the one applied for elastic materials is proposed by Raeisi et al. in [10].

The most notable plastic material properties are yield strength, ultimate strength and tangent modulus. In the case of using different grades of the same material, the yield strength is the most appropriate parameter to be normalized and considered as a variable for ordered SIMP. The yield strength values are mapped between 0 and 1 for the materials of interest. In the case of two completely different materials, the interpolation scheme will have to be applied to the Young's modulus, for the elastic region, and to the yield strength for the plastic region, to produce the *updated* material model for TO. Figure 13 shows the material card generated from properties for two grades of the same material (steel DP 350 and steel DP 700) for the updated material [10].
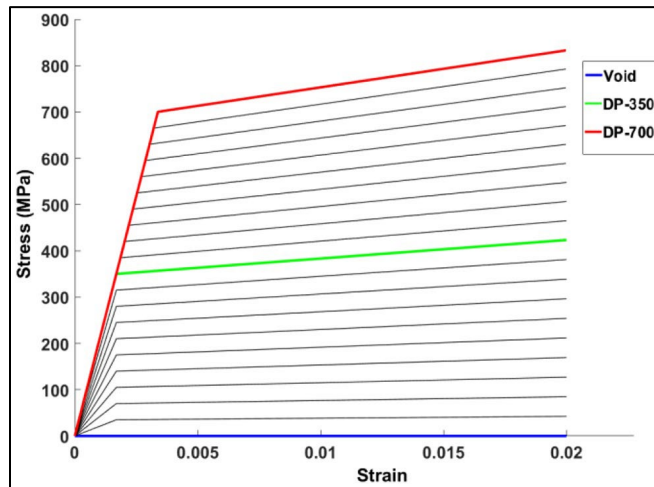

Figure 13: Representation of the material card for Ordered SIMP [10]

$$S_y(\rho_e) = A_s\rho_e^p + B_s, \tag{6}$$

where ρ_e^p is a (penalized) normalized density of the finite element e, with a penalization exponent p. The element densities $\rho_e, e = 1,2, ..., n$, with n being the total number of finite elements, are the design variables for the optimization problem. S_y is the resulting yield strength and the coefficients A_s and B_s for $\rho_e \in [\rho_i, \rho_{i+1}]$ are given as:

$$A_s = \frac{S_y^i - S_y^{i+1}}{\rho_i^p - \rho_{i+1}^p}, \tag{7}$$

$$B_s = E_i - A_E\rho_i^p, \tag{8}$$

where S_i is the yield strength of the ith material.

8 Conclusion and Summary

In this paper, we successfully demonstrated the integration and application of the Ordered SIMP approach with LS-TaSC. The case study demonstrated the application of the ordered SIMP method for interpolating the elastic properties of a material model (in this case piecewise linear elastic-plastic). The methodology described in the paper can also be applied to the plastic region of materials by using the method in Section 7. The ordered SIMP method does not introduce any additional parameters; hence, the computational cost remains the same as the standard SMTO method.

The examples demonstrated that the proposed algorithm can efficiently solve the multi-material topology synthesis problems under multiple loading conditions: static and dynamic. The comparative study between the results obtained from the ordered SIMP approach in LS-TaSC, and the gradient-based methods, indicated the necessity and usefulness of the ordered SIMP interpolation. The case study also showed significant improvement in structural performance of the multi-material design, when compared to the single material designs. Moreover, the finite element simulations with a combination of different materials showed that the responses for both static and crash cases could be tailored by varying individual preferences.

The integration of the ordered SIMP method within LS-TaSC makes it readily accessible to the industry to include such a method into the development process. The approach can also be extended to larger components including a body-in-white (BIW) structure with multiple load cases.

References

[1]   M. Cavazzuti, A. Baldini, E. Bertocchi, D. Costi, E. Torricelli, and P. Moruzzi, "High Performance Automotive Chassis Design: A Topology Optimization based Approach," *Struct. Multidiscip. Optim.*, vol. 44, no. 1, pp. 45–56, 2011.

[2]   M. Bujny, N. Aulig, M. Olhofer, and F. Duddeck, "Identification of Optimal Topologies for Crashworthiness with the Evolutionary Level Set Method," *Int. J. Crashworthiness*, vol. 23, no. 4, pp. 395–416, 2018.

[3]   S. Ramnath, E. Nutwell, N. Aulig, and K. Horner, "Detail Design Evaluation of Extruded Sections on a Body-in-White Concept Model," in *15th International LS-DYNA Users Conference*, 2018.

[4]   E. Raponi, M. Bujny, M. Olhofer, N. Aulig, S. Boria, and F. Duddeck, "Kriging-Assisted Topology Optimization of Crash Structures," *Comput. Methods Appl. Mech. Eng.*, vol. 348, no. 1, pp. 730–752, 2019.

[5]   L. S. Wang, P. Haghighi, S. Ramnath, D. Detwiler, K. Horner, and J. J. Shah, "Automating Parametric Redesign of Structural Thin-Walled Frames," in *ASME 2019 International Design Engineering Technical Conferences & Computers and Information in Engineering Conference*, 2019.

[6]   M. P. Bendsoe and O. Sigmund, *Topology Optimization*. Berlin: Springer, 2004.

[7]   S. Zhou and M. Y. Wang, "Multimaterial structural topology optimization with a generalized Cahn-Hilliard model of multiphase transition," *Struct. Multidiscip. Optim.*, vol. 33, no. 2, pp. 89–111, 2007.

[8]   R. Tavakoli and S. Mohseni, "Alternating active-phase algorithm for multimaterial topology optimization problems: a 115-line MATLAB implementation," *Struct. Multidiscip. Optim.*, vol. 49, no. 4, pp. 621–642, 2013.

[9]   W. Zuo and K. Saitou, "Multi-material topology optimization using ordered SIMP interpolation," *Struct. Multidiscip. Optim.*, vol. 55, no. 2, pp. 477–491, 2017.

[10]   S. Raeisi, P. Tapkir, A. Tovar, C. Mozumder, and S. Xu, "Multi-Material Topology Optimization for Crashworthiness Using Hybrid Cellular Automata," in *SAE Technical Paper Series*, 2019.

[11]   R. Tavakoli, "Multimaterial topology optimization by volume constrained Allen-Cahn system and regularized projected steepest descent method," *Comput. Methods Appl. Mech. Eng.*, vol. 276, pp. 534–565, 2014.

[12]   J. S. Ocampo, "Multi material topology optimization with hybrid cellular automata," Indiana University-Purdue University Indianapolis, 2017.

[13]   A. Tovar, "Bone Remodeling As a Hybrid Cellular Automaton Optimization Process," University of Notre Dame, 2004.

[14]   S. Ramnath, N. Aulig, M. Bujny, S. Menzel, I. Gandikota, and K. Horner, "Load Case Preference Patterns based on Parameterized Pareto-Optimal Vehicle Design Concept Optimization," in *European LS-DYNA Conference*, 2019.

[15]   N. Aulig, E. Nutwell, S. Menzel, and D. Detwiler, "Preference-Based Topology Optimization for Vehicle Concept Design with Concurrent Static and Crash Load Cases," *Struct. Multidiscip. Optim.*, vol. 57, pp. 251–266, 2017.

[16]   N. Aulig, S. Ramnath, E. Nutwell, and K. Horner, "Design Domain Dependent Preferences for Multi-Disciplinary Body-in-White Concept Optimization," in *15th International LS-DYNA Users Conference*, 2018.